SUPPLEMENTARY MATERIAL:
Large-scale free-space photonic circuits in two dimensions

Maria Gorizia Ammendola,[1,2,*] Francesco Di Colandrea,[1,3,†] Lorenzo Marrucci,[1,4] and Filippo Cardano[1,‡]

[1] *Dipartimento di Fisica, Università degli Studi di Napoli Federico II, Complesso Universitario di Monte Sant'Angelo, Via Cintia, 80126 Napoli, Italy*
[2] *Scuola Superiore Meridionale, Via Mezzocannone, 4, 80138 Napoli, Italy*
[3] *Nexus for Quantum Technologies, University of Ottawa, K1N 5N6, Ottawa, ON, Canada*
[4] *CNR-ISASI, Institute of Applied Science and Intelligent Systems, Via Campi Flegrei 34, 80078 Pozzuoli (NA), Italy*

SUPPLEMENTARY DATA

We provide experimental results for different input coin-polarization states. Figures **S1**-**S2**-**S3** show the probability distributions obtained for a $|H\rangle$, $|V\rangle$, and $|L\rangle$ polarization input state (cf. Fig. 3), respectively. Figure **S4** shows the QW ballistic spreading for the same polarization inputs (cf. Fig. 4(d)).

To demonstrate the versatility of our method, we compute the optic-axis patterns of the 3 LCMSs that would be needed for the simulation of 3, 5, 10, and 20 time steps of an alternative split-step QW protocol: $U_{ss} = T_y(\delta = \pi/2)WT_x(\delta = \pi/2)W$, where T_x, T_y and W are the lattice and coin operators introduced in the manuscript. We also simulate the output field intensity for a localized $|H\rangle$-polarized input state and compare it with the theoretical QW probability distribution. The results are reported in Fig. **S5**.

* MGA and FDC contributed equally to this work.

† francesco.dicolandrea@unina.it
‡ filippo.cardano2@unina.it

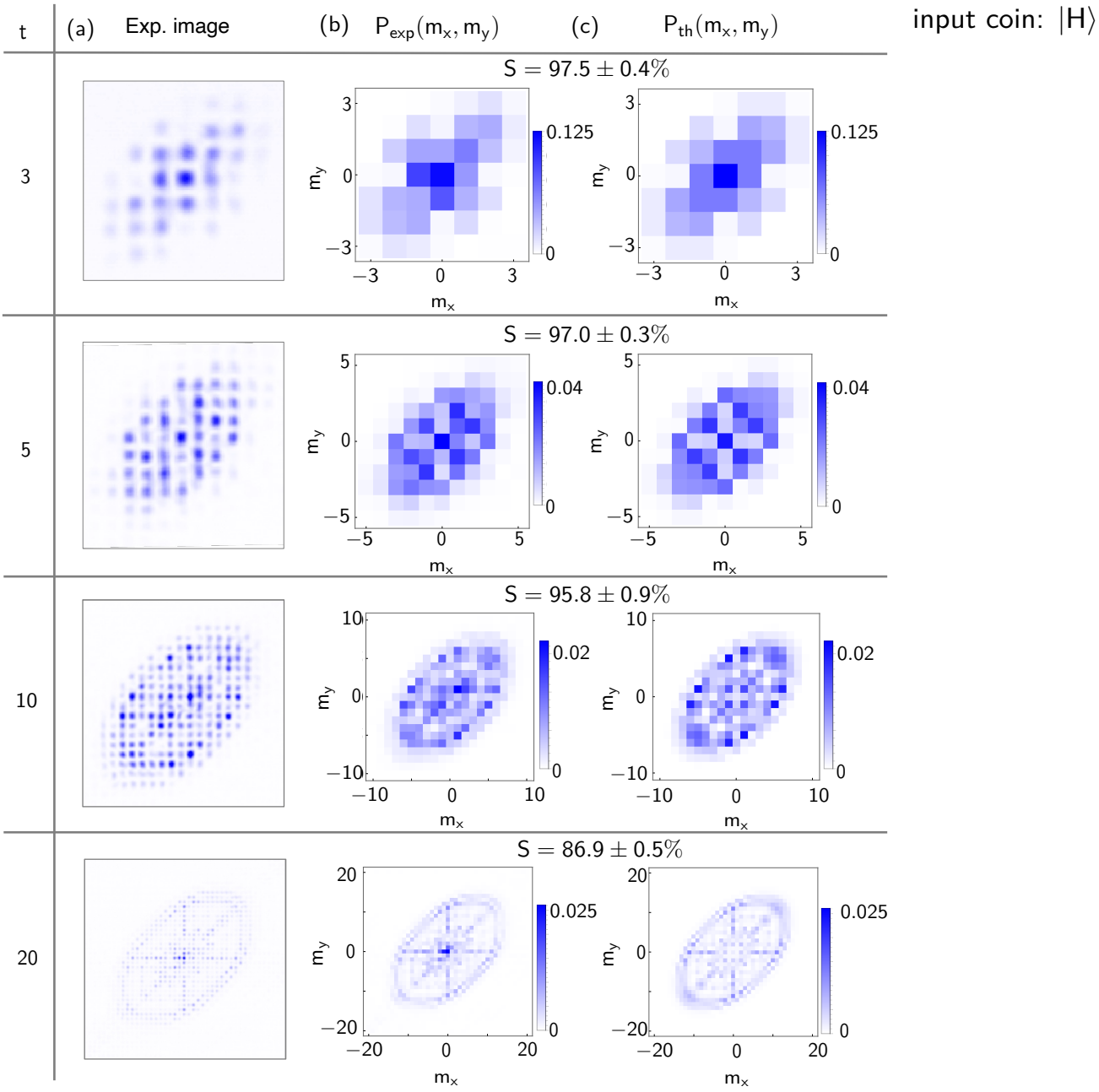

Figure S1. 2D QWs via spin-orbit photonics. (a) Experimental images obtained for a $|H\rangle$-polarized input state, from which the walker probability distribution $P_{\rm exp}(m_x, m_y)$ is extracted (b), and compared with the theoretical prediction $P_{\rm th}(m_x, m_y)$ (c). For each realization, we report the value of the similarity, computed as the average of four independent measurements. The rows refer to 3, 5, 10, and 20 time steps (t), respectively.

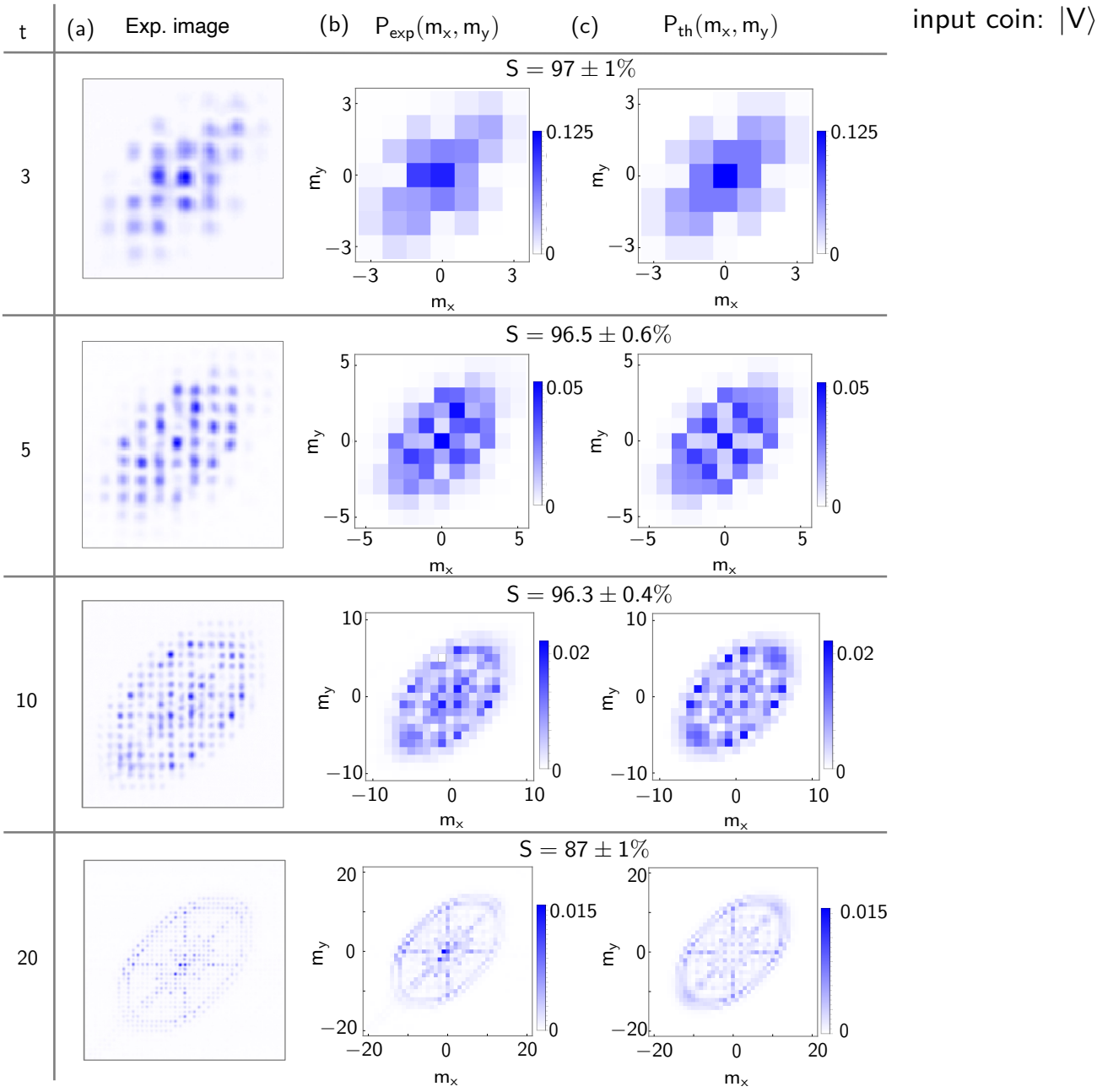

Figure S2. 2D QWs via spin-orbit photonics. (a) Experimental images obtained for a $|V\rangle$-polarized input state, from which the walker probability distribution $P_{\rm exp}(m_x, m_y)$ is extracted (b), and compared with the theoretical prediction $P_{\rm th}(m_x, m_y)$ (c). For each realization, we report the value of the similarity, computed as the average of four independent measurements. The rows refer to 3, 5, 10, and 20 time steps (t), respectively.

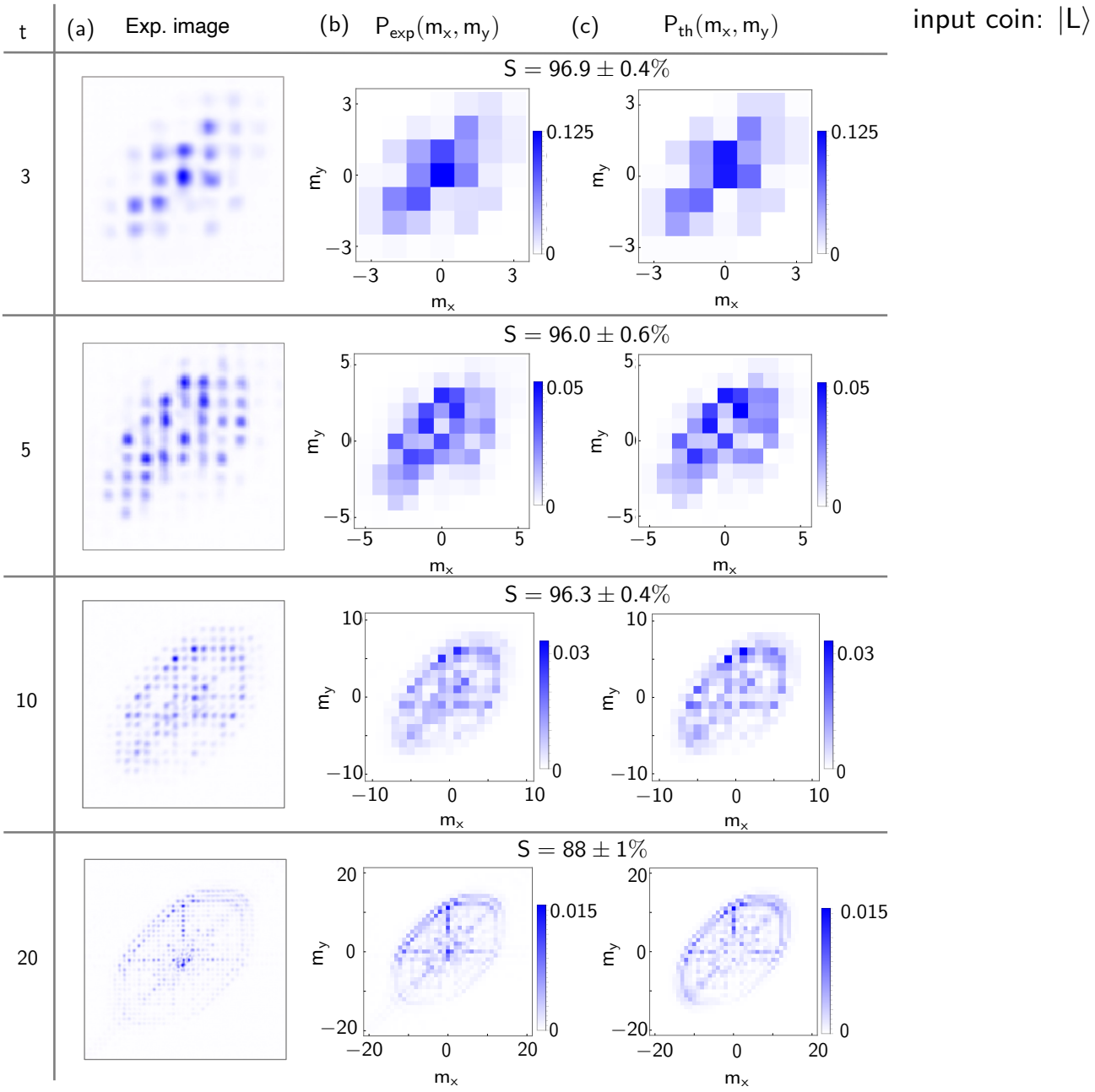

Figure S3. **2D QWs via spin-orbit photonics.** (a) Experimental images obtained for a $|L\rangle$-polarized input state, from which the walker probability distribution $P_{\rm exp}(m_x, m_y)$ is extracted (b), and compared with the theoretical prediction $P_{\rm th}(m_x, m_y)$ (c). For each realization, we report the value of the similarity, computed as the average of four independent measurements. The rows refer to 3, 5, 10, and 20 time steps (t), respectively.

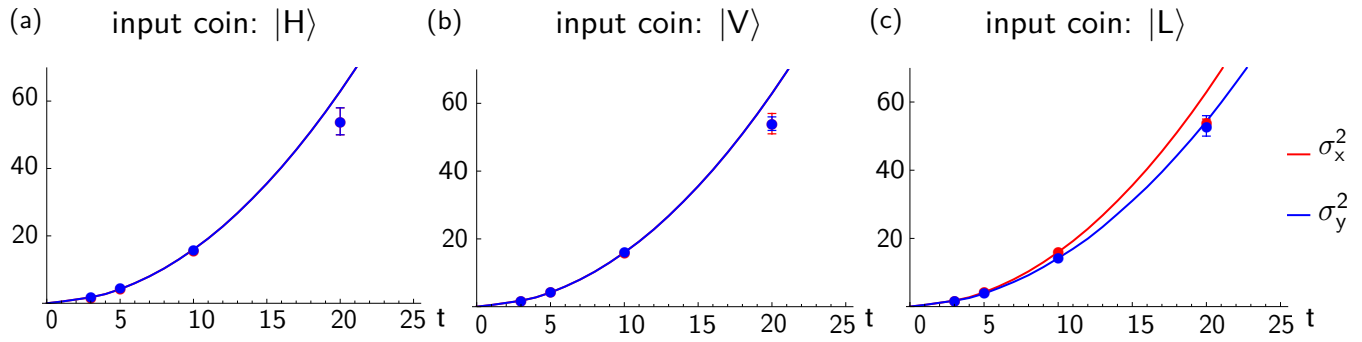

Figure S4. Variance of 2D QW distributions. Variance of the output distribution along x and y, σ_x^2 and σ_y^2, for different input states: (a) $|H\rangle$, (b) $|V\rangle$, (c) $|L\rangle$. The experimental points (dots) correctly reproduce the expected ballistic behavior (solid lines) extracted numerically.

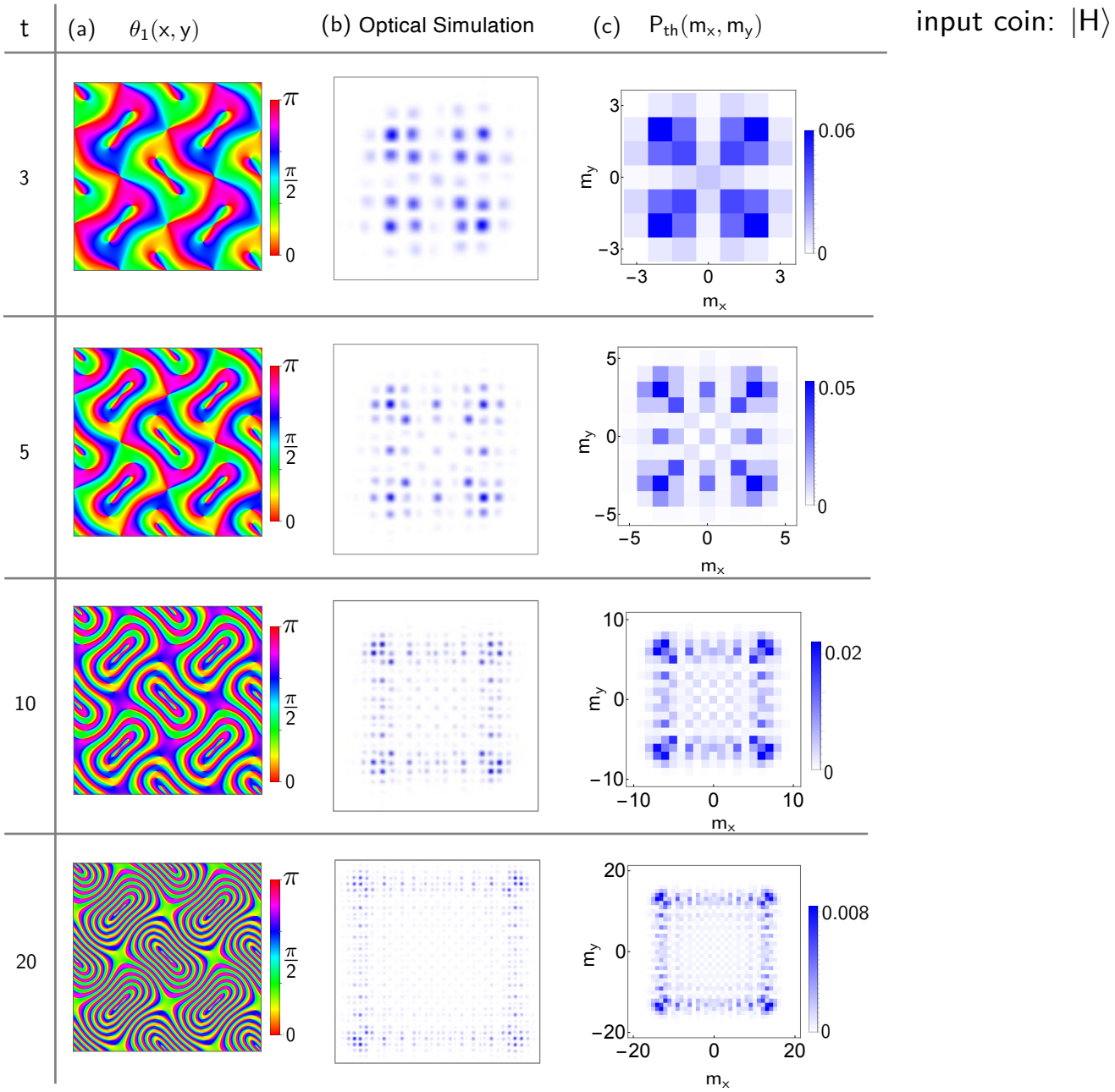

Figure S5. Split-step 2D QW with LCMSs. (a) Computed optic-axis modulation of the first metasurface ($\theta_1(x, y)$) for the simulation of a split-step 2D QW at different time steps (t). (b) Simulation of the output field intensity for a $|H\rangle$-polarized input, compared with the theoretical prediction (c) $P_{\text{th}}(m_x, m_y)$.